frontiers in Remote Sensing

ORIGINAL RESEARCH
published: 30 March 2022
doi: 10.3389/frsen.2022.860282

Applying a Multi-Method Framework to Analyze the Multispectral Acoustic Response of the Seafloor

Pedro S. Menandro[1]*, *Alex C. Bastos*[1], *Benjamin Misiuk*[2] and *Craig J. Brown*[2]

[1]Marine Geosciences Lab, Departamento de Oceanografia e Ecologia, Universidade Federal do Espírito Santo, Vitória, Brazil, [2]Seascape Ecology and Mapping Lab, Department of Oceanography, Dalhousie University, Halifax, NS, Canada

Improvements to acoustic seafloor mapping systems have motivated novel marine geological and benthic biological research. Multibeam echosounders (MBES) have become a mainstream tool for acoustic remote sensing of the seabed. Recently, "multispectral" MBES backscatter, which is acquired at multiple operating frequencies, has been developed to characterize the seabed in greater detail, yet methods for the use of these data are still being explored. Here, we evaluate the potential for seabed discrimination using multispectral backscatter data within a multi-method framework. We present a novel MBES dataset acquired using four operating frequencies (170, 280, 400, and 700 kHz) near the Doce River mouth, situated on the eastern Brazilian continental shelf. Image-based and angular range analysis methods were applied to characterize the multifrequency response of the seabed. The large amount of information resulting from these methods complicates a manual seabed segmentation solution. The data were therefore summarized using a combination of dimensionality reduction and density-based clustering, enabling hierarchical spatial classification of the seabed with sparse ground-truth. This approach provided an effective solution to synthesizing these data spatially to identify two distinct acoustic seabed classes, with four subclasses within one of the broader classes, which corresponded closely with seafloor sediment samples collected at the site. The multispectral backscatter data also provided information in likely, unknown, sub-surface substrate differences at this site. The study demonstrates that the adoption of a multi-method framework combining image-based and angular range analysis methods with multispectral MBES data can offer significant advantages for seafloor characterization and mapping.

Keywords: seabed classification, multispectral backscatter, density-based clustering, seafloor mapping, benthic habitat mapping, multibeam echosounder

OPEN ACCESS

Edited by:
DelWayne Roger Bohnenstiehl, North Carolina State University, United States

Reviewed by:
Luis A. Conti, University of São Paulo, Brazil
Bishwajit Chakraborty, Council of Scientific and Industrial Research (CSIR), India

***Correspondence:**
Pedro S. Menandro
pedromenandro@gmail.com

Specialty section:
This article was submitted to Acoustic Remote Sensing, a section of the journal Frontiers in Remote Sensing

Received: *22 January 2022*
Accepted: *14 March 2022*
Published: *30 March 2022*

Citation:
Menandro PS, Bastos AC, Misiuk B and Brown CJ (2022) Applying a Multi-Method Framework to Analyze the Multispectral Acoustic Response of the Seafloor. Front. Remote Sens. 3:860282. doi: 10.3389/frsen.2022.860282

1 INTRODUCTION

Technological innovations have advanced many areas of marine science over the past several decades, including seafloor mapping. Improvements to acoustic seafloor mapping systems have motivated novel benthic geological and biological research. Recently, seabed mapping science has led to the development of a number of seabed classification tools (Fonseca et al., 2009; Rzhanov et al., 2012; Lecours et al., 2016; Ierodiaconou et al., 2018; Masetti et al., 2018), which facilitate multidisciplinary approaches to environmental management and conservation (Cogan et al.,

2009; Lee et al., 2015; Kirkman et al., 2019) across a range of different scientific disciplines (Heap et al., 2014; Mosca et al., 2016; Brooke et al., 2017).

Over the last 2 decades, multibeam echosounders (MBES) have become a mainstream tool for acoustic remote sensing of the seabed (Brown et al., 2011; Menandro and Bastos, 2020). MBES are now widely used for hydrographic purposes and applied research on the continental shelf (Innangi et al., 2015; Rocha et al., 2020) and deep sea (Sen et al., 2016; Picard et al., 2018; Stewart and Jamieson, 2019). In addition to measuring bathymetry, acoustic backscatter can be recorded from the MBES signal. The concept of backscatter is basically the acoustic energy that returns from the seabed to the receiver of the sonar (Lurton, 2010), while it is still very complex structurally, following absorption, reflection, and scattering of the signal by the seabed and water column, and influence of physical properties such as the acoustic frequency and the angle of incidence. Backscatter strength measurements have proven highly useful for discriminating benthic habitats (e.g., Costa, 2019; Harris and Baker, 2020; Trzcinska et al., 2020) and surficial geology (McGonigle and Collier, 2014; Montereale-Gavazzi et al., 2018). Most MBES backscatter seabed mapping analyses can be divided into two domains: 1) image-based analyses, whereby backscatter data are compensated for angular dependence and analyzed as a single raster image (e.g., Diesing et al., 2016; Ierodiaconou et al., 2018; Runya et al., 2021) and 2) angular range analysis, in which the full angular response of backscatter is retained (Fonseca and Mayer, 2007; Fonseca et al., 2009; Haris et al., 2011; Lurton et al., 2018). Angle-varying gain (AVG), which is used to produce the mosaic for image-based approaches, generally results in a loss of angular resolution, meaning that information may be lost that is specific to individual angles of incidence at the seafloor. Angular range analysis, on the other hand, may be used to preserve angular detail at the cost of spatial resolution. Fonseca et al. (2009) point out that angular response and backscatter mosaic analysis can be considered as complementary methods, and the improvement of benthic maps through combined approaches has been demonstrated (Che Hasan et al., 2012; Che Hasan et al., 2014).

Currently, most MBES operate at a single acoustic frequency, despite acknowledgement that the backscatter response of the seafloor is frequency dependent. The difference between single- and multi-frequency backscatter analysis is comparable to mono- and multi-frequency optical remote sensing (Diesing et al., 2016). The field of terrestrial remote sensing is well developed with a fairly long history, and advanced models for image classification using optical data employ a wide range of electromagnetic frequencies simultaneously to achieve a more robust description of the land surface (Lu and Weng, 2007). Multi-frequency (aka, "multispectral") acoustic remote sensing of the seafloor, in contrast, it is not yet as developed—though the potential advantages of multispectral acoustic data have been recognized (Huges Clarke, 2015; Tamsett et al., 2016; Feldens et al., 2018). The recent implementation of multispectral MBES allows for bathymetry and backscatter acquisition at multiple frequencies simultaneously. Buscombe and Grams (2018), Gaida et al. (2018), Brown et al. (2019), and Costa (2019) investigated and presented the first results of multispectral MBES operating in this manner. These studies reported improved seafloor discrimination as a result of the multifrequency dataset, which provides increased information enabling detailed comparison of acoustic signatures between different seabed types.

Despite these apparent advantages, the use of multifrequency MBES for seafloor characterization is not well developed in many contexts. For example, single frequency backscatter datasets from both sidescan and MBES systems are useful as exploratory survey tools to obtain baseline knowledge of the composition of the seafloor (Augustin et al., 1996; Greene et al., 2013; Lucieer et al., 2018). Because of the increased information they provide, multifrequency systems may be well suited to exploratory tasks, yet the use of multiple frequencies also implies an increase in dimensionality that must be resolved to realize the full benefit of these data. Additionally, several techniques may be used to derive secondary backscatter features for seafloor characterization, for example, by analyzing the acoustic angular response of the seafloor or the texture of the backscatter image (e.g., Blondel and Sichi, 2009; Alevizos and Greinert, 2018; Fakiris et al., 2019). While highly useful for classification, these approaches also serve to increase the dimensionality of the data, and this effect is multiplicative in a multifrequency context. Furthermore, it is not immediately clear which of these approaches or which information should be prioritized for exploratory purposes, especially where there is little a priori knowledge on the composition of the seafloor or sparse ground truth coverage.

Building on previous work, here we evaluate the potential for seabed discrimination using multispectral backscatter data within a multi-method exploratory framework. We first present a novel MBES dataset acquired using four operating frequencies (170, 280, 400, and 700 kHz), with ground truth sediment information. Adopting a geoacoustic approach, image-based and angular range analysis methods are applied to characterize the multifrequency response of the seabed. The large amount of information resulting from these methods is then summarized using dimensionality reduction and density-based clustering, enabling hierarchical spatial classification of the seabed with sparse ground-truth.

2 MATERIALS AND METHODS

2.1 Data Acquisition and Processing

The current study focuses on a seafloor area (37 km^2) adjacent to the Doce River mouth, situated on the eastern Brazilian continental shelf, in the state of Espírito Santo. The Doce River is one of the main river deltas recognized along the Brazilian eastern coast (Dominguez, 2006), and is a major sediment source to the adjacent continental shelf (Bastos et al., 2015). In terms of sedimentary processes, Quaresma et al. (2015) characterized a deltaic lobe extending to 30 m depth, with an accumulation of fine sediments (>75% mud) in a main depocenter south from the river mouth. Towards offshore (depths >30 m), sandy facies are predominant (**Figure 1**)—a trend also observed and corroborated by Vieira et al. (2019). Though useful, previous research in this area has been conducted

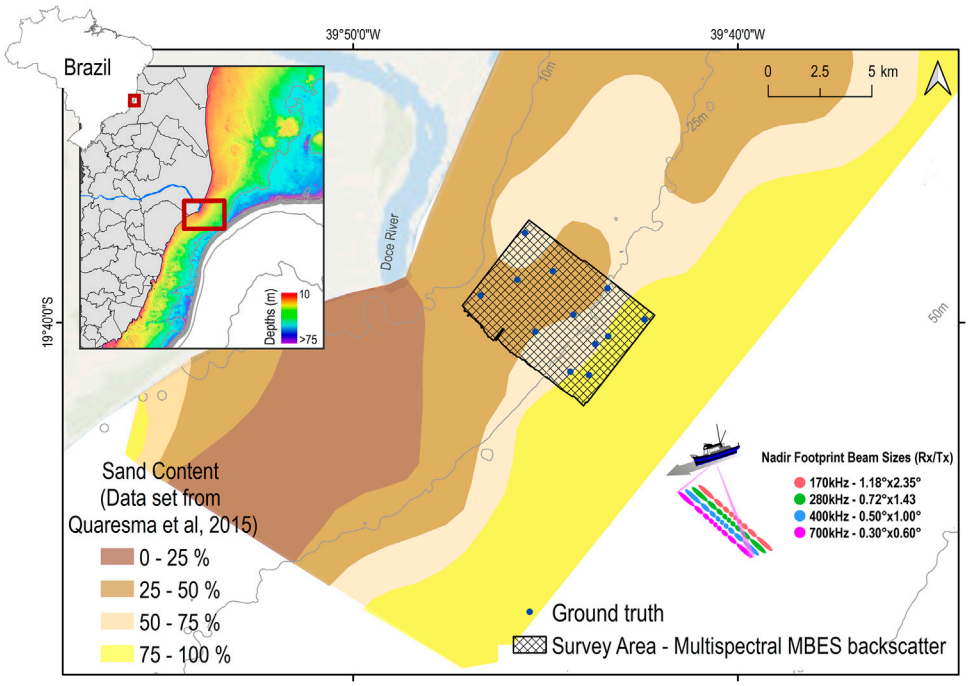

FIGURE 1 | Map of the study area (bathymetry adapted from Bastos et al., 2015), with sand content estimated by Quaresma et al. (2015). On the right-hand side, an illustration of multispectral MBES acquisition indicates frequency changes between sequential pings, and the nadir beam footprint sizes for each frequency.

at a coarse spatial resolution, and fine scale geomorphological and substrate characterization are still lacking. The MBES and sediment sample data sets presented here were analyzed to fill this knowledge gap.

A multispectral MBES dataset was acquired to provide high resolution information on the geomorphology and substrate distribution of the study area. Bathymetry and backscatter were acquired using an R2Sonic 2024 echosounder, with the sonar head deployed through a moon pool in the steel-hulled survey vessel, "Santa Edwiges" (19.6 m in length). The MBES was configured to collect data by sequentially pinging at 170, 280, 400, and 700 kHz (true frequency of 697.674 kHz) operating frequencies in equiangular mode. The 700 kHz frequency did not operate during the entire survey due to the effects of depth and water turbidity on data quality. Specifications such as power, pulse length, gain, and spreading were held constant. A 90° angular sector and 256 beams were used for all frequencies except 700 kHz, which is limited to a 70° sector. Because the receiver array is flat, the size of the receive beam grows with distance from nadir (i.e., the lower the grazing angle, the larger the beam footprint; **Figure 1**). The transmit array is round and does not suffer the same issue.

The MBES system was paired with a POS MV Wave Master Inertial Navigation System (INS), with differential positioning. During the survey, SVP casts were deployed every 3 hours using a Valeport Mini configured to collect sound velocity, salinity, temperature, and pressure. These data are essential to ensure the correction of sound velocity effects and to calculate and apply the absorption coefficient. Application of absorption coefficients for each frequency was the only radiometric correction applied during the data acquisition—all other corrections (e.g., beam width) were applied during post processing. All systems were integrated using QPS QINSy 8.18.3 for data acquisition, and the survey lines were planned with ~30% overlap. The dataset was assessed during the survey to ensure data quality using QPS Qimera 2.0, and post-processing was carried out using QPS Qimera and QPS FMGT 7.9.5 (Fledermaus Geocoder Toolbox, hereafter FMGT).

In compliance with the International Hydrographic Organization, bathymetric processing consisted of manually cleaning erroneous soundings and tidal correction, which was performed using data extracted from an ADCP moored adjacent to the study area. The dataset was filtered for each operating frequency in QPS Qimera. Digital bathymetric models (DBM) for each frequency were exported at a 2 m horizontal resolution.

Although there is still no unified standard for processing backscatter, the multispectral data were processed following recommendations in Lamarche and Lurton (2018) and Schimel et al. (2018). The main steps involve the frequency filtering, correction of acquisition parameters for each frequency (gain, transmit power, pulse length, beam width) and AVG correction. Backscatter mosaics were exported at 1 m resolution. All backscatter processing was completed using FMGT.

2.2 Multispectral Backscatter Analysis

Elements of both image-based and angular range approaches were used to analyze backscatter data and explore the

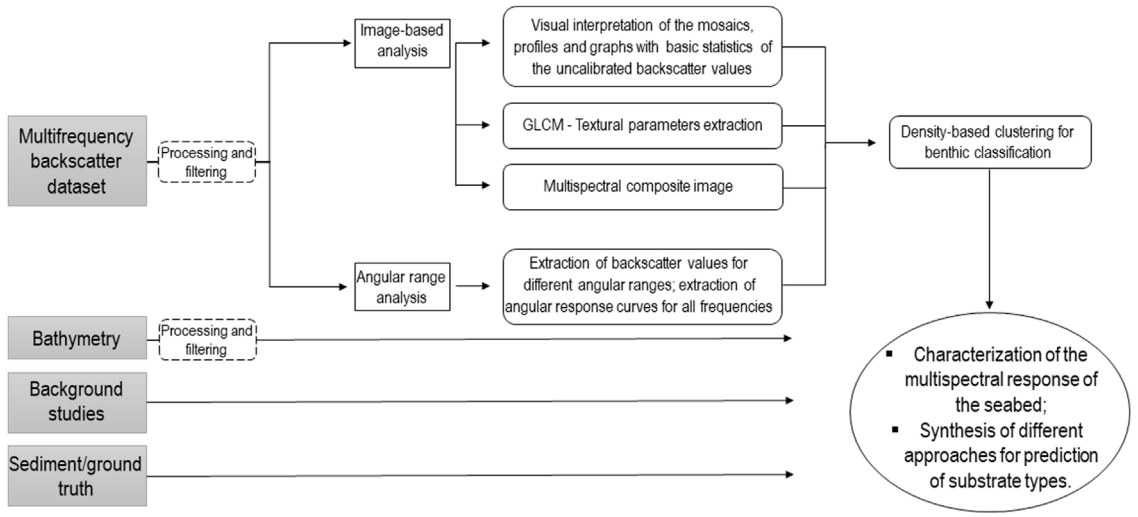

FIGURE 2 | Flow indicating the steps of the methodological framework.

multispectral response of the seabed. The methodological framework of the analysis is summarized in **Figure 2**, outlining each approach and its expected results.

2.2.1 Image-Based Analysis

The image-based analysis can be subdivided into three steps. The first step consists of visual interpretation of the mosaics and assessment of the uncalibrated backscatter values for each frequency using profiles, graphs, and descriptive statistics. This step is critical for obtaining baseline understanding of the data and is often combined with other analyses (Parnum and Gavrilov, 2011). General data exploration and visual comparisons were performed using ArcGIS and R. In the second step, textural parameters were extracted from the mosaics, which is a common technique for classifying acoustic data (Diesing et al., 2016; Diesing et al., 2020). Here, textural analyses were based on grey-level co-occurrence matrices, using the GLCM v 1.6.5 package available in R (Haralick et al., 1973). For each mosaic, GLCM variance measurements were extracted, based on how frequently different combinations of neighboring pixels occur (in a 5x5-pixel window). The third step was the generation of a multispectral composite image (i.e., a false-colour RGB) using each frequency as a spectral band. This approach has not yet been widely applied, likely as a function of the recent development of multispectral MBES, but has great potential to improve habitat discrimination in combination with other terrain attributes.

2.2.2 Angular Range Analysis

The second approach applied to the multifrequency corrected backscatter dataset was angular range analysis (ARA). The backscatter angular dependence (the acoustic response across the range of ensonification grazing angles), provides information that can be used for improved seabed classification (Che Hasan et al., 2014; McGonigle and Collier, 2014; Fezzani and Berger, 2018), or the inference of seafloor physical properties such as grain size and acoustic impedance (Fonseca and Mayer, 2007). Fonseca et al. (2009) suggested that the angular response curve can be sectorized according to the angular range—comprising, for example, the near range region (near nadir) from 0 to 25°, the far range region from 25 to 55°, and the outer range region from 55 to 85°. Angular response curves were extracted at each ground truth sample site through swath profiles for comparison with geophysical models and comparison between frequencies. Additionally, corrected and georeferenced soundings were extracted from FMGT outputs for each 10° sector from the nadir (i.e., 1°–10°, 11°–20°, 21°–30° and 31°–40°) using a custom R script. These results were rasterized and integrated with the layers from with other approaches within ArcGIS for further analysis.

2.3 Density-Based Clustering

The large amount of information from the different analysis approaches (*Multispectral Backscatter Analysis*) was summarized spatially using density-based clustering. Unlike many clustering methods that rely on measures of multivariate distance to identify clusters, these approaches identify clusters using estimates of multivariate data density (Hahsler et al., 2019; Hashler and Piekenbrock, 2021). Density-based clustering offers several advantages compared to many other approaches, such as the automatic identification of cluster numbers, rejection of outliers that do not fall within any dense regions, and clustering of data of arbitrary multivariate shape (Ester et al., 1996; Kriegel et al., 2011). Ordering Points to Identify Clustering Structure (OPTICS) is a method that can additionally identify clusters of varying density (Ankerst et al., 1999). OPTICS is an extension of the DBSCAN algorithm (Ester et al., 1996), which facilitates data exploration through "reachability plots"—one-dimensional representations of the "reachability distance" between points (Hahsler et al., 2019). These can be used to inform the clustering outcome, and enable additional flexible solutions such as hierarchical density-based clustering. Despite the widespread application of unsupervised approaches for seabed

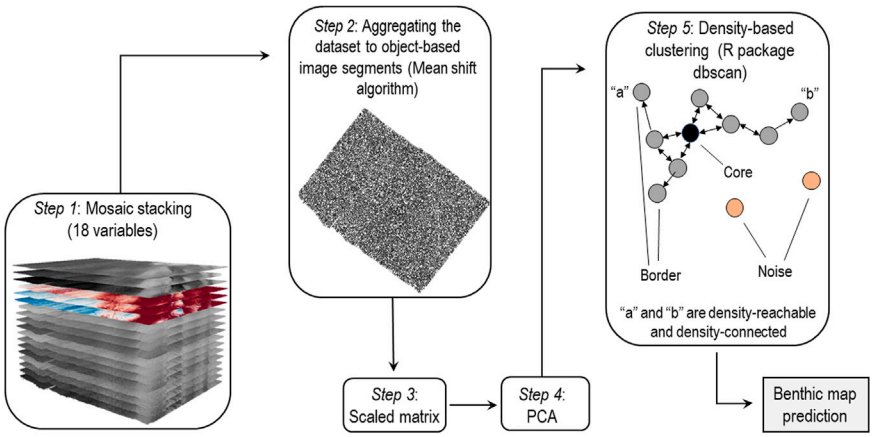

FIGURE 3 | Workflow for density-based clustering of the highly dimensional multi-method backscatter analysis. Illustrative scheme of density-based clustering was adapted from Hahsler et al. (2019).

mapping and classification, and the potential benefits offered by density-based clustering, it has received relatively little attention in this field (but see Le Quilleuc et al., 2021).

Results from both image-based and angular range approaches were used for clustering, with the exception of the frequency of 700 kHz, which has a smaller coverage area and was not considered for this analysis. These layers included AVG backscatter mosaics for each frequency (170, 280, and 400 kHz), GLCM variance for each frequency (170, 280, and 400 kHz), and backscatter values from four different angular sectors (1–10°, 11–20°, 21–30°, 31–40°) for each frequency (170, 280 and 400 kHz), totaling 18 rasters (3 AVG mosaics, 3 rasters from GLCM results, and 12 rasters from ARA). We applied the methods presented in Che Hasan et al. (2012) in order to aggregate the acoustic data to object-based image segments. The three-band RGB backscatter mosaic was segmented using the "mean shift" algorithm (Yizong, 1995; Comaniciu and Meer, 2002) in ArcGIS Pro using the maximum spatial and spectral detail, but a minimum segment size of 2000 pixels. The mean shift is a "mode-seeking" algorithm that assigns data points to clusters based on their position relative to the local maxima of a multivariate kernel density estimate. The values of the 18 rasters were stacked and averaged over the resulting segments, which allowed for continuous estimates of the angular backscatter values across the full extent of the study area, and a reduction of data volume by several orders of magnitude, producing 6902 segments (step 2 of **Figure 3**). The values for each segment (18 acoustic variables) were converted to matrices in R, and principal component analysis (PCA) was applied to eliminate collinearity and reduce dimensionally. The first two components explained 95.4% of the total variance and were retained for clustering.

Principal components of the image-based segments were clustered using OPTICS to identify acoustically distinct seabed types across the study area. OPTICS was implemented using the DBSCAN package in R (**Figure 3**; Ester et al., 1996, Campello et al., 2013; Hahsler et al., 2019). The reachability distance was first plotted using the parameters (the density search radius) and (a threshold number of points used for reachability calculations) to visualize the data density and estimate the number of clusters. The reachability plot suggested a hierarchical data structure, and two sets of clusters were extracted at coarse and fine levels of detail. These indicated broad data groupings, which contained smaller sub-clusters at a higher level of detail. The clustering results were exported to GIS format to generate benthic map predictions.

2.4 Ground Truth Information

After preliminary analysis of the backscatter mosaics, samples of surficial sediments were collected at 12 sites within the survey area (**Figure 1**). Sediments were collected using a Van Veen grab sampler in July 2021 (nearly 2 years after the acoustic data survey). To account for the temporal offset between the collection of sediment samples and acoustic data, we verified the differences and the general trend from the sediment distribution (Quaresma et al., 2015; Vieira et al., 2019). The grain size analysis provides results as percentage gravel, coarse sand, medium sand, fine sand, silt and clay, which were used to ground-truth results from the multiple backscatter analysis approaches and density-based clustering.

3 RESULTS

3.1 Multispectral Bathymetry

The DBM outputs, which contain all processed depths from all frequencies combined, ranged from 10 to 32 m, and revealed a predominantly flat bottom with locally steep features. These were evident in maps of local slope and roughness, and ridges oblique to the coast were visible at the deep end of the profile (**Figure 4**).

The spatial distribution of depth differences was also investigated. DBM surfaces generated for each operating frequency were subtracted from each other using raster algebra to visualize the distribution of depth differences across the study area (**Figure 5**). In general, regions close to

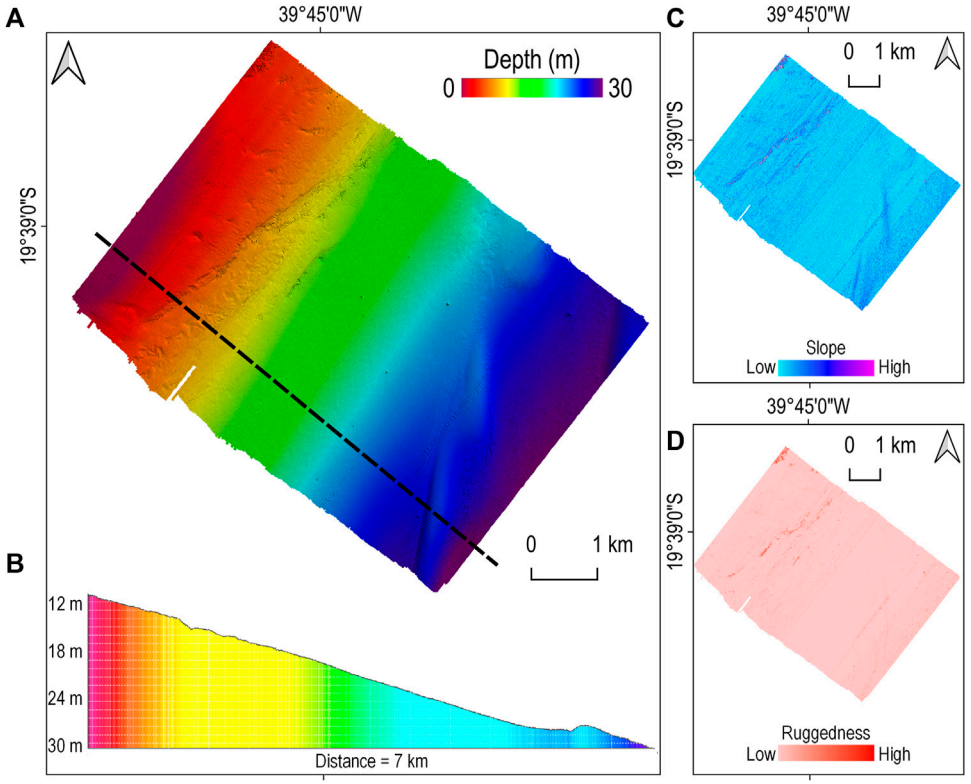

FIGURE 4 | (A) Digital bathymetric model; **(B)** bathymetric profile; **(C)** slope; **(D)** ruggedness.

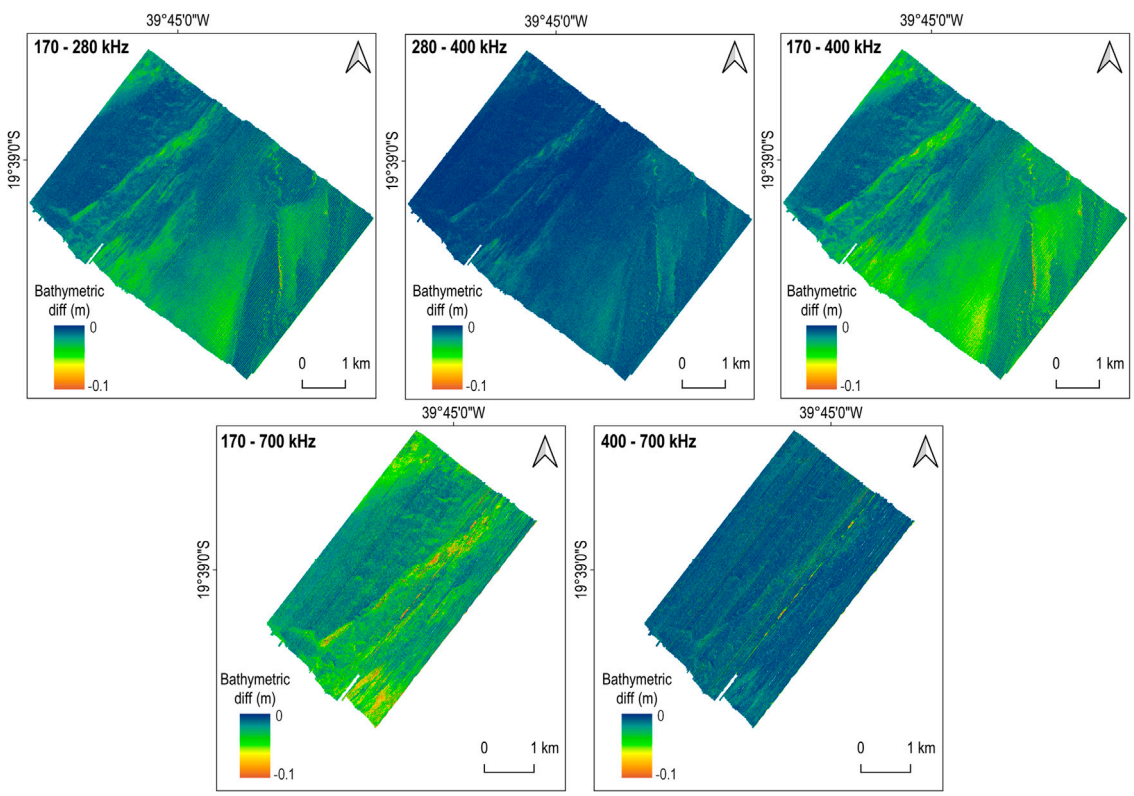

FIGURE 5 | Bathymetric difference surfaces (in meters) computed from the subtraction between the digital bathymetric models of each frequency.

higher slope values (steep feature and the edges of oblique ridges) show higher bathymetric difference between frequencies. Differences between 170 and 280 kHz were, on average, 0.1 m greater than the differences between 280 and 400 kHz, and differences between 170 and 400 kHz were greater still. The differences between 700 and 170 kHz were the greatest observed, whereas differences between 400 and 700 kHz were three times lower. The bathymetric differences (which can reach up to 0.2 m) observed between the frequencies largely conformed to expectation given the current understanding of substrate-frequency response and the bottom type in the study area.

3.2 Multispectral Backscatter

3.2.1 Image-Based Analysis

3.2.1.1 Assessment of Mosaics and Uncalibrated Backscatter Values

Figure 6 presents the uncalibrated backscatter mosaics for each frequency at 1 m resolution using the same range of values for the greyscale (−10 and −38 dB). Overall, the shallower region presents the lower backscatter values, and the oblique elongated bathymetric features correspond with higher backscatter values.

From visual analysis, differences between the frequencies appear greater in low backscatter regions, while over the high backscatter feature running south-north through the survey area all frequencies show high backscatter values, and differences are not apparent (**Figures 6**, **7**). The 700 kHz mosaic appeared oversaturated. **Figure 7** suggests a general trend of increasing backscatter and greater agreement between frequencies with increasing distance from northwest to southeast across the survey area.

Uncalibrated backscatter values for the frequencies of 170, 280 and 400 kHz were plotted as violin plots for the whole area (**Figure 8A**) and also for all frequencies using only the 700 kHz coverage area (**Figure 8B**). These plots present the kernel probability density of the data. Considering the entire area, the lowest median backscatter values (−30.63 dB) were observed using the 400 kHz frequency. The 170 kHz backscatter median was greater (−24.97 dB), with the smallest interquartile range of values (between Q1 and Q3), which is also reflected in the concentration of data observed in the kernel density curve with leptokurtic tendency and positive asymmetry (see **Figure 8B**). The 280 kHz data presented a higher median value (−26.54 dB) than the 400 kHz, and both frequencies presented similar data distributions (**Figure 8A**), recognizing two distinct sets of backscatter values (the main one having a modal value close of −27.80 dB for 280 kHz and −31.89 dB for 400 kHz). The better recognition of two main groups of

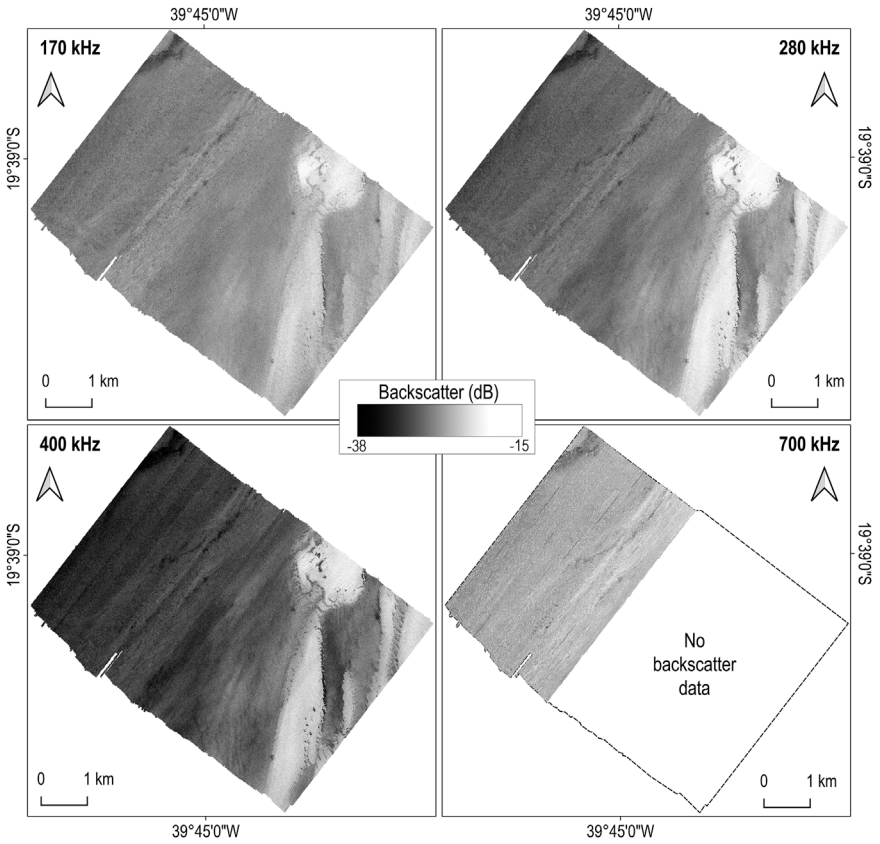

FIGURE 6 | Backscatter mosaics for each operating frequency.

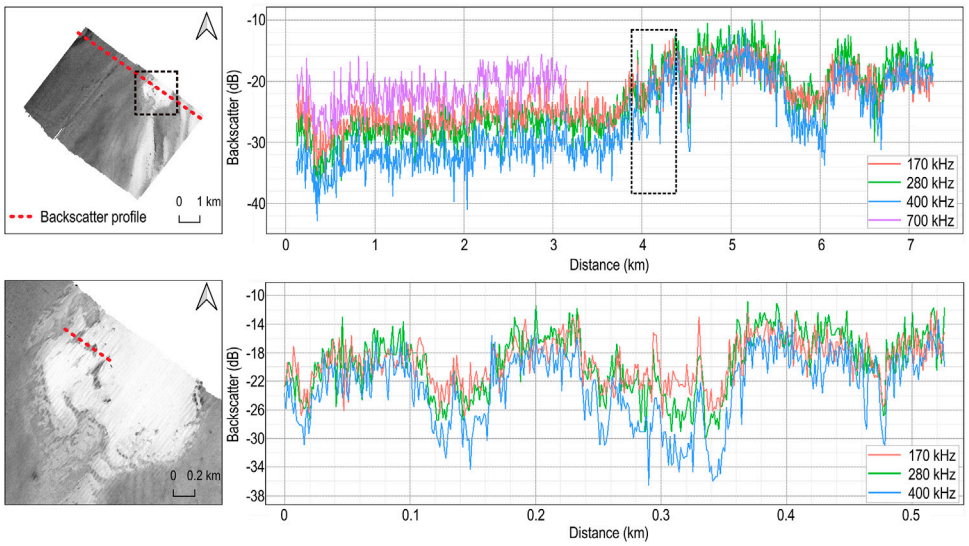

FIGURE 7 | Top: comparison of differences in multispectral backscatter intensities along the transect shown in the mosaic (top left). Bottom: comparison of differences in multispectral backscatter intensities along the transect shown in the mosaic inset (bottom left).

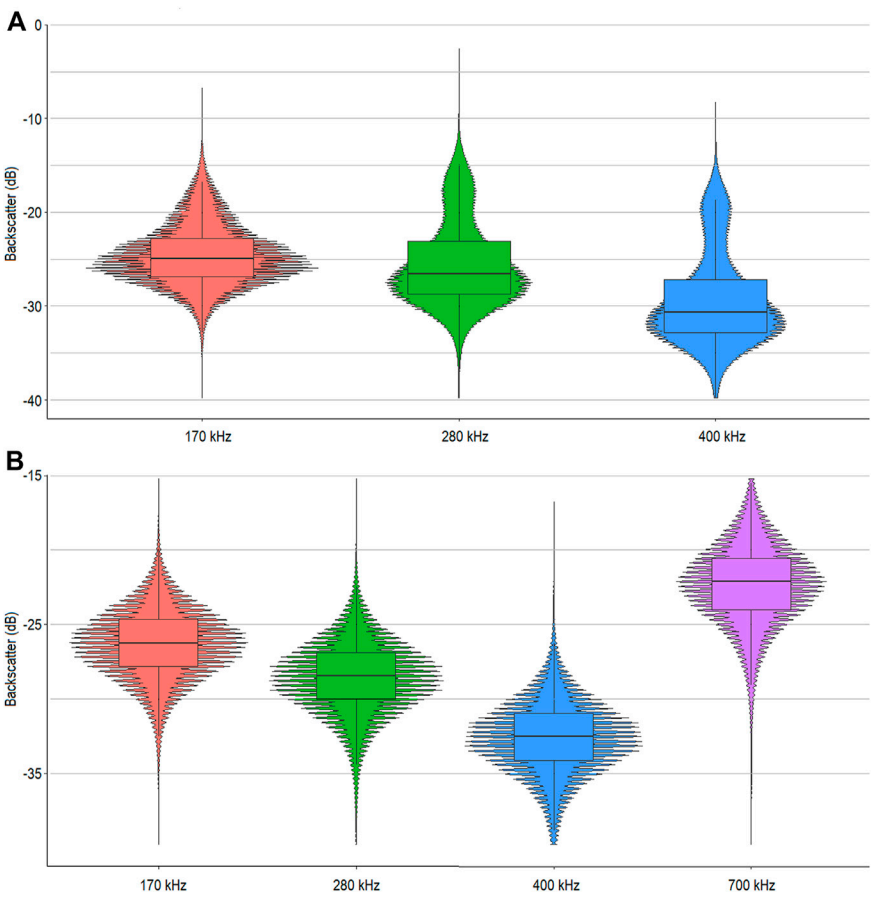

FIGURE 8 | (A) Violin plots presenting backscatter data (170, 280, and 400 kHz) for the whole area, and **(B)** for all frequencies, spatially restricted within the 700 kHz coverage area.

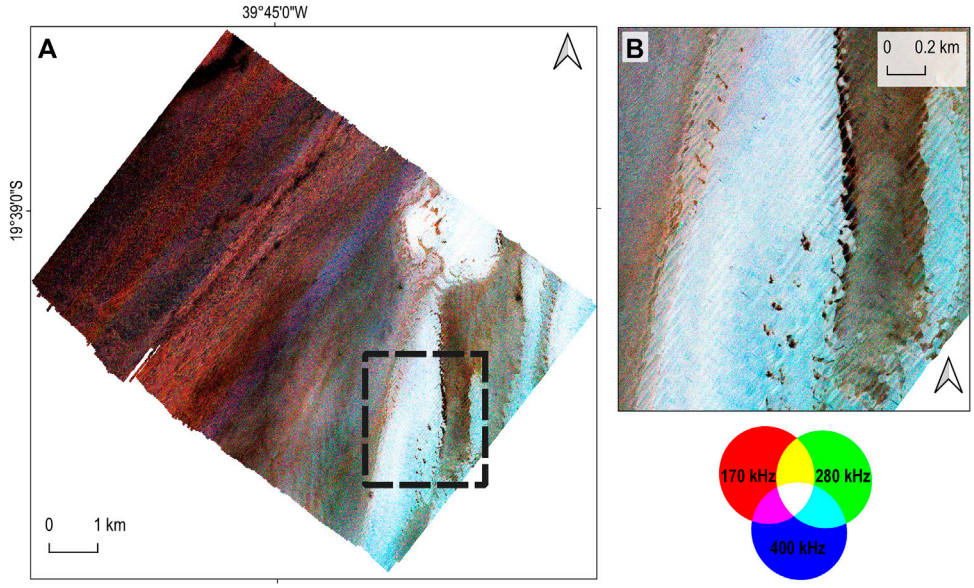

FIGURE 9 | Composite image (RGB) representing the three frequencies **(A)** For the whole study area; **(B)** Frame over the sandy feature. Pixels are stretched to the minimum and maximum values for each band. No changes of color rendering parameters were applied (hue, saturation and contrast).

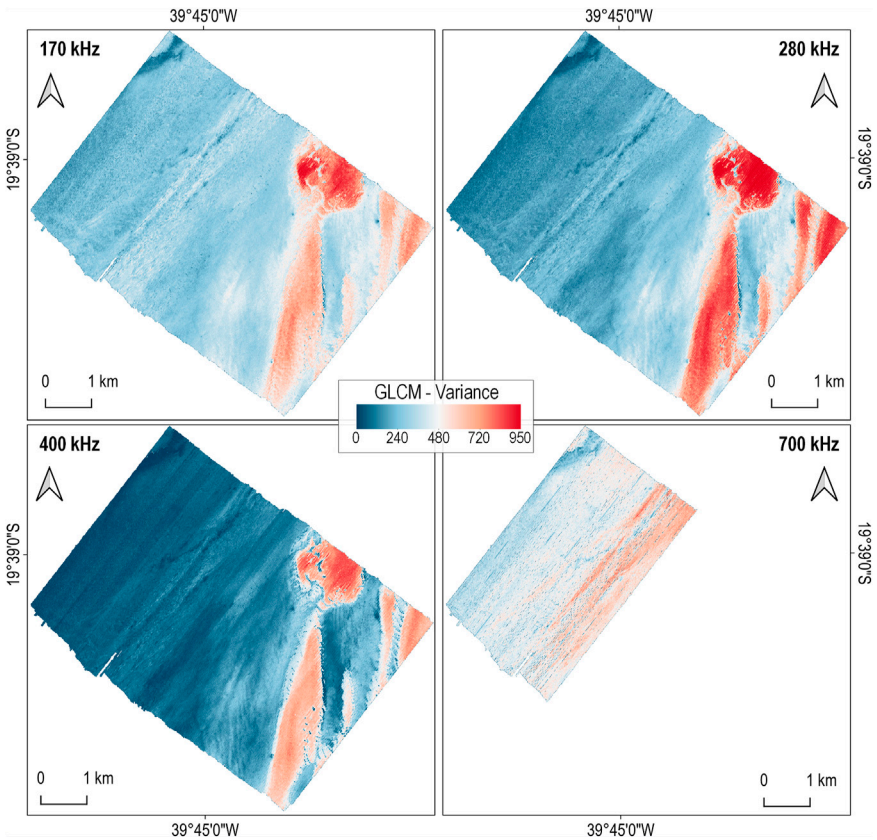

FIGURE 10 | GLCM variance results for each frequency.

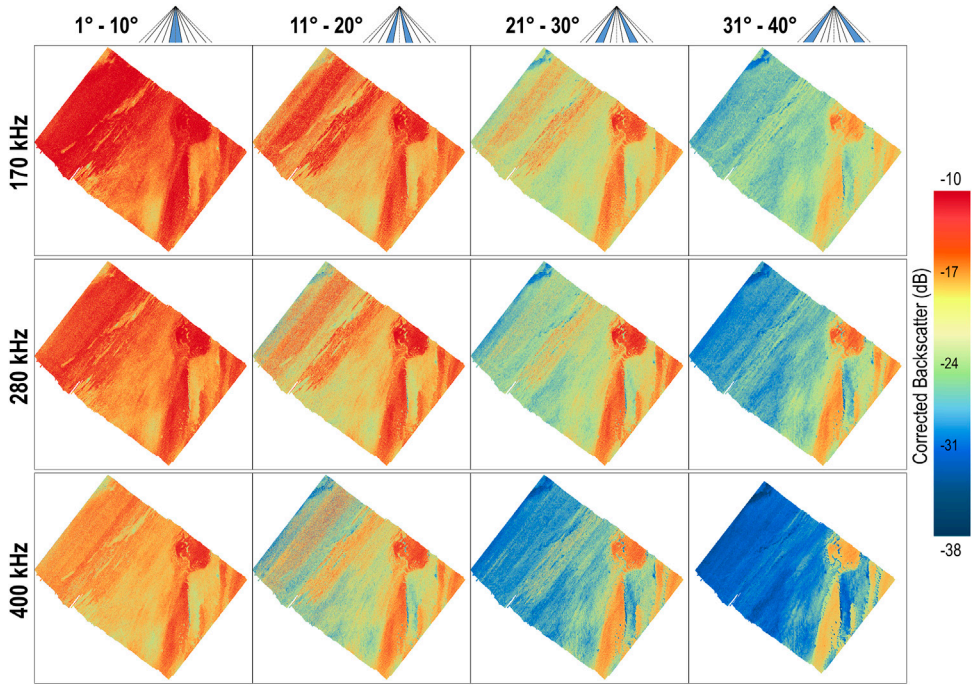

FIGURE 11 | Angular range analysis results obtained by extraction of backscatter values for each 10° angular sector.

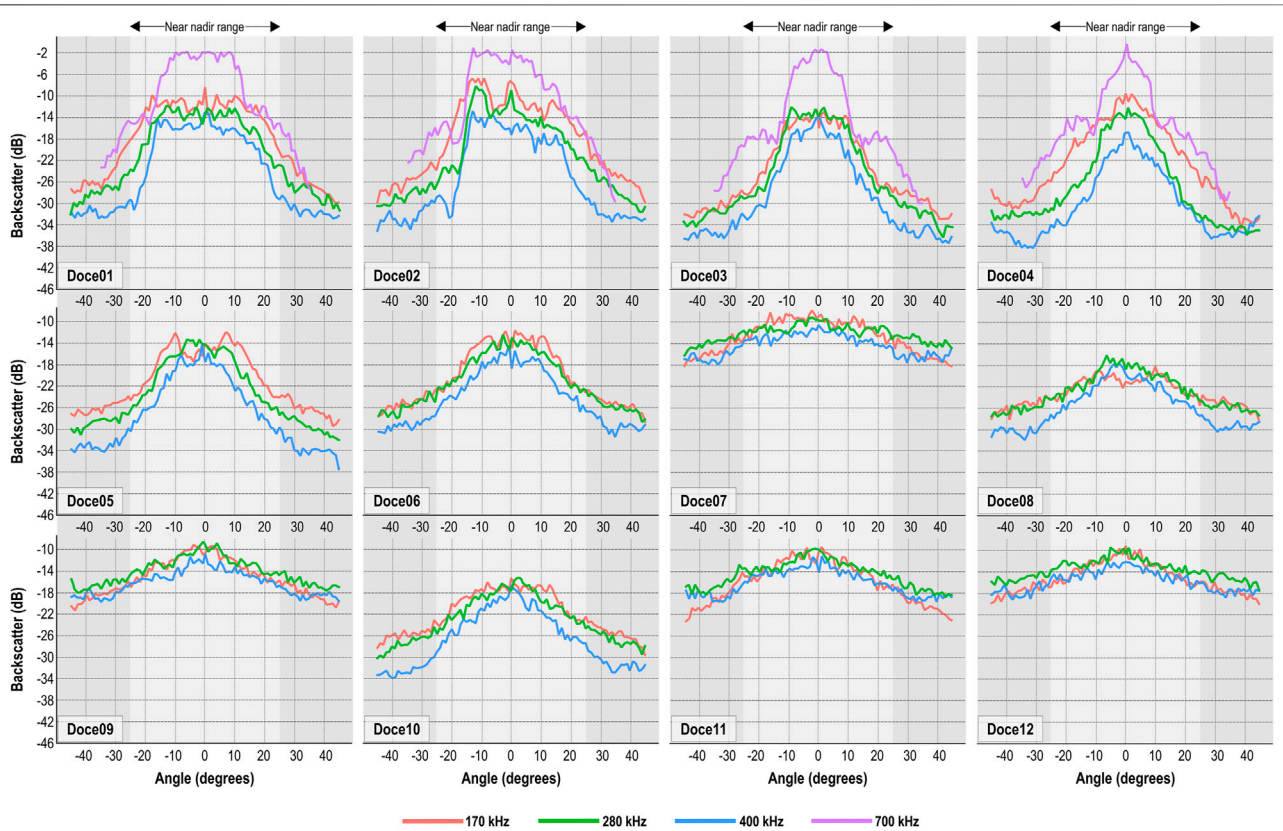

FIGURE 12 | Angular dependence curves for each frequency extracted in each sample site.

backscatter values by the higher frequencies can also be observed by the standard deviation of the dataset for each frequency (170 kHz: 3.35 dB, 280 kHz: 4.64 dB, 400 kHz: 5.09 dB).

Over the 700 kHz coverage (**Figure 8B**), the lowest median backscatter values (−33 dB) were observed for the 400 kHz data. The similar shape of the density curves (**Figure 8B**) is expected, once the seabed appears to be more homogeneous in this area in accordance with visual analysis of the mosaics. Considering the oversaturated mosaic, and that little is currently known concerning the acoustic response of 700 kHz frequency, we reserve a detailed image-based interpretation of the 700 kHz data. Further investigation would be useful to inform on the effects of a turbid water column on such high-frequency MBES soundings.

3.2.1.2 Multispectral Composite Image

The backscatter mosaics were combined to produce a three-band composite RGB image (**Figure 9**). In the RGB mosaic, it is possible to recognize zones where all frequencies show similarly high backscatter values (white regions), which coincide with the elongated and oblique features. Darker zones indicate low backscatter values for all frequencies. The greatest differences between the bands are indicated by red shades, which indicates higher values for the 170 kHz signal, and in light blue areas, which indicate higher values for the combination of the two higher frequencies (280 and 400 kHz).

3.2.1.3 Textural Analysis (GLCM)

The general trend of textural variations can be visualized using the GLCM variance (**Figure 10**). Higher values occurred over the high backscatter feature, especially at 280 kHz. Lower values occurred in the low backscatter region, mainly at 400 kHz.

3.2.2 Angular Range Analysis

The angular range analysis provides results that can be explored using geophysical and empirical approaches, including physical model comparison and empirical parameters to distinguish seafloor types, and also angular dependence curves of different substrates (Lurton and Lamarche, 2015). The angular backscatter values were interpolated spatially using Inverse Distance Weighting (IDW) in ArcGIS Pro to produce grids of 1 × 1 m

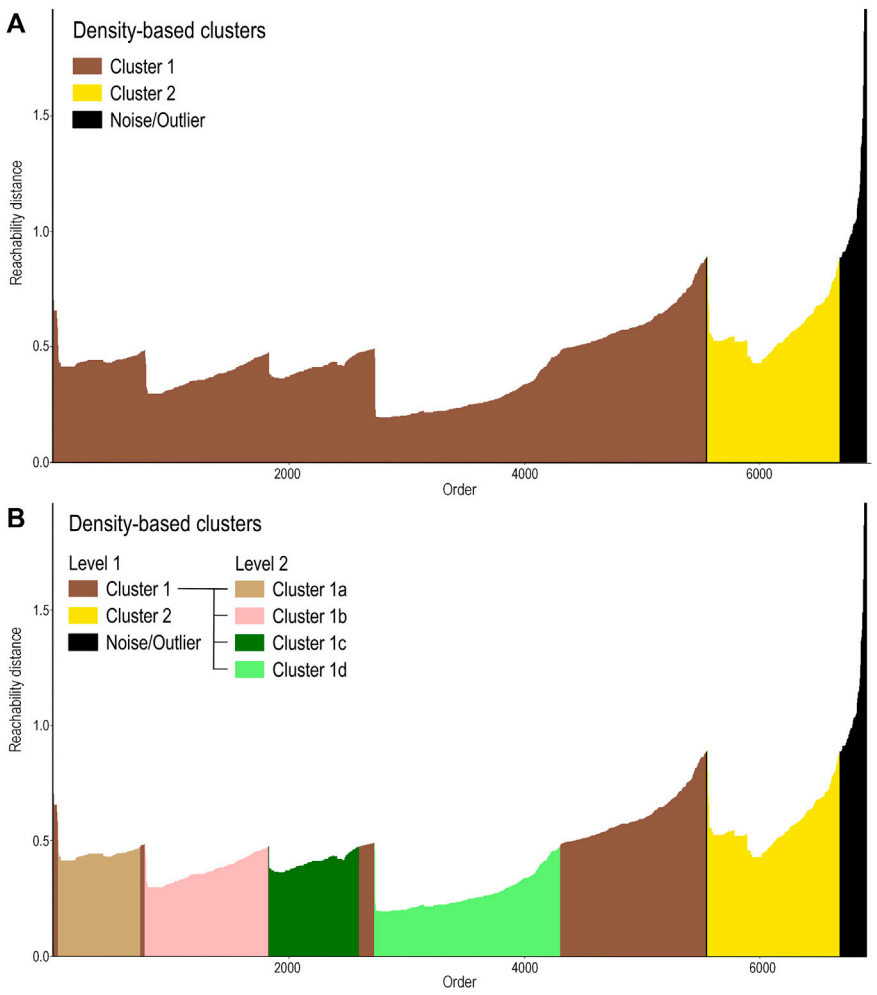

FIGURE 13 | Reachability plot of a hierarchical clustering with **(A)** two main clusters (reachability distance = 0.88) and noise; and **(B)** clusters at detailed hierarchical level (reachability distance = 0.475).

cells (**Figure 11**). The results demonstrated that, for most of the area, decreasing backscatter was associated with increased incidence angle and frequency. The exception occurs over the high-backscatter feature, which marks a region with high scattering across the entire swath.

The 1–10° sector shows high backscatter values throughout the area and similar results for all frequencies. Compared to results presented for the lower frequencies at 11–20° sector, the 400 kHz frequency seems to achieve a better power of seafloor discrimination for the shallower region. Three distinct regions are clearly visible using the 21–30° sector. Additionally, the 400 kHz data within this sector may suggest that the shallow region is composed of different material than the elongated feature, even though they appear similar at other frequencies and angular sectors. Lower backscatter was observed using the outermost angular sector over much of the study area—primarily at 400 kHz—but high values were still observed at the elongated feature.

Angular response curves were extracted for all frequencies to characterize the acoustic response of the seabed at each sample site (**Figure 12**). The angular response curves can be broadly described in three main groups. The curves at sample sites Doce 01 and Doce 02 show similar shapes for all frequencies, with decreasing backscatter values as the frequency increases (with exception of 700 kHz). The shape shows low backscatter level loss for the first 20° from the nadir, followed by a greater decrease in backscatter with increasing incidence angle. The curves extracted at Doce 07, 09, 11, and 12 are comparatively flat, with high backscatter values and very slight differences between frequencies. The third group is characterized by a high backscatter level loss for all frequencies from nadir to the outer beams, and lower values at 400 kHz.

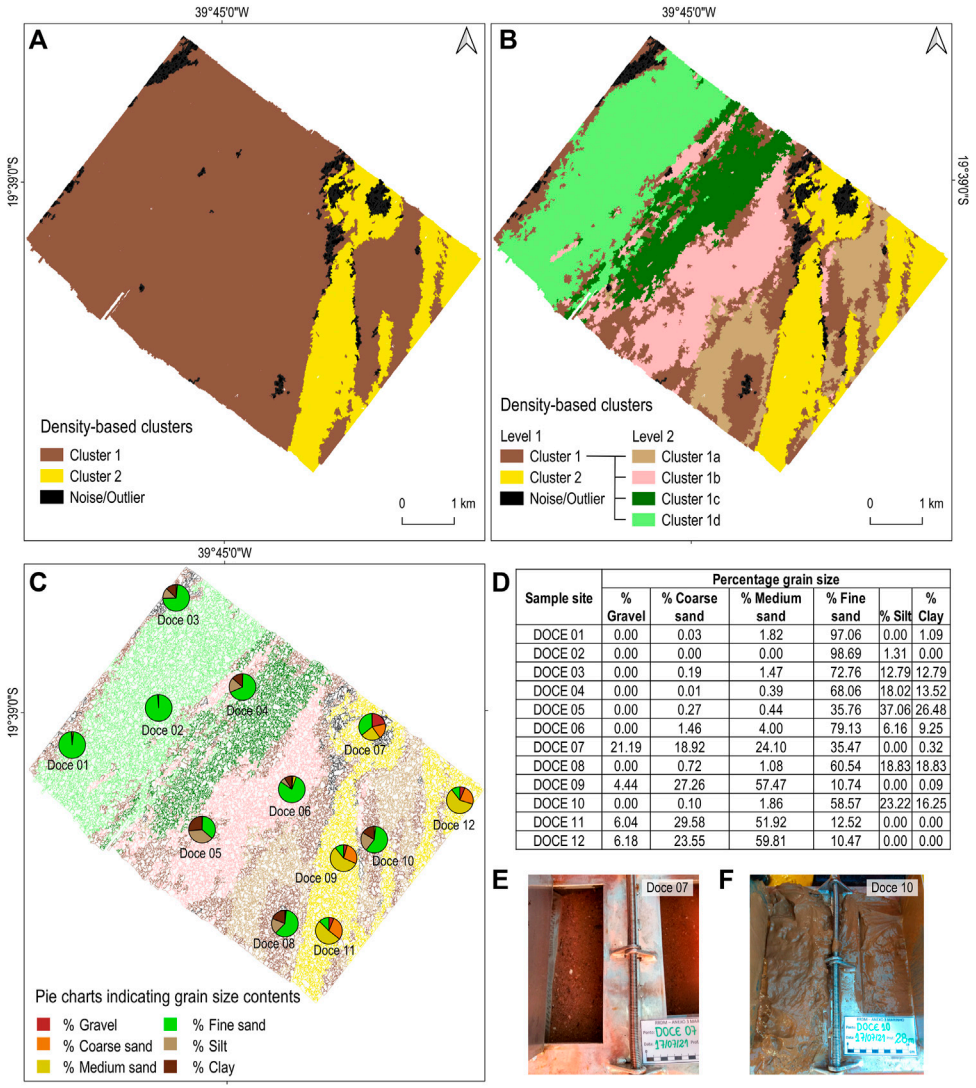

Sample site	Percentage grain size					
	% Gravel	% Coarse sand	% Medium sand	% Fine sand	% Silt	% Clay
DOCE 01	0.00	0.03	1.82	97.06	0.00	1.09
DOCE 02	0.00	0.00	0.00	98.69	1.31	0.00
DOCE 03	0.00	0.19	1.47	72.76	12.79	12.79
DOCE 04	0.00	0.01	0.39	68.06	18.02	13.52
DOCE 05	0.00	0.27	0.44	35.76	37.06	26.48
DOCE 06	0.00	1.46	4.00	79.13	6.16	9.25
DOCE 07	21.19	18.92	24.10	35.47	0.00	0.32
DOCE 08	0.00	0.72	1.08	60.54	18.83	18.83
DOCE 09	4.44	27.26	57.47	10.74	0.00	0.09
DOCE 10	0.00	0.10	1.86	58.57	23.22	16.25
DOCE 11	6.04	29.58	51.92	12.52	0.00	0.00
DOCE 12	6.18	23.55	59.81	10.47	0.00	0.00

FIGURE 14 | (A) Density-based clusters predicting for the study area showing two main clusters; **(B)** clusters at detailed hierarchical level; **(C)** grain size results on top of clustering solution; **(D)** results of each grain size fraction for each sample; **(E)** sediment sample at Doce 07 sample site; **(F)** sediment sample at Doce 10 sample site.

TABLE 1 | Characteristics of each cluster.

	Ground truth samples	Angular response curve	Sediment properties
Cluster 1	Doce 04, 05, 08 and 10	High backscatter level loss	Mostly mud or fine sand
Cluster 1a	—	—	—
Cluster 1b	Doce 06	High backscatter loss	Predominantly fine sand, with more than 10% mud
Cluster 1c	—	—	—
Cluster 1d	Doce 01 and 02	Increased backscatter loss past 20°	More than 95% fine sand
Cluster 2	Doce 09, 11 and 12	Low backscatter loss	Predominantly medium sand, with less than 10% gravel
Noise/Outlier	Doce 03 and 07	High (Doce 03) and low (Doce 07) BS level loss	Fine sand with less than 30% mud (Doce 03) and gravelly sand (Doce 07)

3.3 Density-Based Clustering and Mapping

The combination of PCA and density-based clustering enabled synthesis of a large number of backscatter data layers to inform seabed classification. PCA reduced the 18 backscatter-derived layers to two principal components that explained the majority of variance (>95%) in the dataset, suggesting substantial collinearity among the variables. The OPTICS reachability plot from these principal components (**Figure 13**) enabled identification of clusters at two hierarchical levels. Low reachability distances, represented as valleys in the plot, indicate dense data regions, which are separated by "peaks" representing regions of low data density. First, two broad, well-defined clusters were evident at a reachability distance of 0.88 (**Figure 13A**). These results agree with general trends observed for many of the backscatter layers (**Figures 6**, **10**, **11**), in which the study area is separable into distinct areas of low and high backscatter intensity and variance. Cluster 1, which occurred across the full extent of the study area (**Figure 14A**), could be further divided at a reachability distance of 0.48 to produce four sub-clusters. Unlike the broader Cluster 1, the four sub-clusters show a distinct gradient from the coast (**Figure 14B**), which was not immediately apparent from visual analysis of the various backscatter layers. Outliers appear in regions of extreme high and low backscatter values.

3.4 Grain Size

The results from grain size analysis (**Figures 14C,D**) show that samples Doce 01 and Doce 02 are composed primarily of fine sand. Doce 03 and Doce 04 share a similar mud content and both stations are close to bathymetric anomalies (high slope and high ruggedness sites). Samples Doce 05, Doce 08 and Doce 10 (**Figure 14F**) had an increased mud content, while sample sites at the high backscatter features (Doce 07, 09, 11, 12) - e.g., **Figure 14E** - had higher proportions of medium and coarse sand fractions, with low amounts of mud.

Although there not enough samples to estimate the classification accuracy, the classes seem to distinguish benthic clusters through the multivariate combination of the results. **Table 1** summarizes the main properties for each cluster defined.

Cluster 1 contained the greatest number of sediment samples and can be characterized as muddy fine sand. Cluster 2 is medium sand, with a smaller coarse sand fraction. Cluster 1a contains no ground truthing validation, but seems to indicate a transition between clusters 1 and 2. Cluster 1b seems to have characteristics close to cluster 1a, likely with higher mud content, or morphological characteristics that provide a soft backscatter response. Cluster 1c also does not have sediment samples, but it can be interpreted as similar to cluster 1b, according to the angular sector maps (**Figure 11**). Cluster 1d has two samples and can be defined as fine sand. Some areas were left unclassified but may comprise two additional substrate types—one with higher coarse sand/gravel contents (sample Doce 07) and the other with extremely low backscatter values, indicating a muddy bottom. It is possible that the latter has undergone modifications during the time between the collection of acoustic data and ground truthing.

4 DISCUSSION

Backscatter data has been analyzed in a variety of ways for seafloor classification, including interpretation of backscatter mosaics, textural analysis (Runya et al., 2021), image-based analysis (Ierodiaconou et al., 2018), and techniques involving angular range analysis (Fonseca and Mayer, 2007). Advantages and disadvantages of each make the choice of methodology challenging, and their combined use may achieve better results by uniting the spatial resolution of the mosaics with the enhanced information supplied from angular analysis (Fonseca et al., 2009; Che Hasan et al., 2014). Several supervised and unsupervised techniques have been applied in seabed classification (Stephens and Diesing, 2014; Diesing et al., 2020) and incorporated in segmentation algorithms, including different clustering approaches (Le Bas, 2016; Masetti et al., 2018). Density-based clustering has received little attention for seabed classification, and was successfully applied here to synthesize different analysis approaches to produce a classified output.

4.1 Benthic Map Prediction

Highly dimensional input data resulting from multiple analysis approaches can be difficult to synthesize spatially, especially given sparse ground truth information, yet density-based clustering provides an objective means to identify well-defined seabed units under such circumstances. Here, backscatter mosaics (**Figure 6**) and the composite RGB (**Figure 9**) potentially suggest two or three seabed classes, while the angular response curves at the 12 sample sites (**Figure 12**) suggest at least three classes. GLCM products and spatial analysis of different angular sectors further confound a unified manual seabed segmentation solution. The combination of image-based segmentation, dimensionality

reduction, and density-based clustering provide an objective solution to synthesizing these data spatially to identify distinct seabed types. Similar solutions have applied PCA for dimensionality reduction of backscatter data followed by k-means clustering for unsupervised classification (e.g., Alevizos et al., 2018), and other approaches towards similar ends have included combinations of self-organizing maps and fuzzy clustering (Chakraborty et al., 2015), and Bayesian probability estimation (Amiri-Simkooei et al., 2009; Simons and Snellen, 2009). Several properties of density-based clustering are desirable in an exploratory context though, including automatic identification of number of clusters, enhanced data visualization and hierarchical clustering solutions, and rejection of outliers that are dissimilar from other well-defined clusters. These qualities are lacking in many other common approaches, which may be well-suited to classifying gradational or poorly defined seabed types (e.g., k-means, ISO, agglomerative clustering).

Quantifying the advantages of using multispectral backscatter data as a predictor for different seafloor types is beyond the scope of the current study, but the findings suggested that the multifrequency acoustic data provided greater discrimination of muddy and fine sand sediments than coarser sediments, aligned with findings from other studies (Gaida et al., 2018; Brown et al., 2019; Costa, 2019). Part of the data identified as noise by the OPTICS algorithm is located in the region of highest backscatter, where the sediment shows the higher gravel and coarse sand content. Conversely, multiple distinct clusters were identifiable in muddy sediments. We believe this to be a property of the acoustic data, which were highly variable and inhomogeneous at the high backscatter regions. Further investigations using multispectral backscatter for a greater range of seabed types is necessary to determine the potential of this technology for substrate discrimination. This is also the first application of density-based clustering methods in this context as far as we know, and further comparison with other clustering methods in various environments would be of great interest.

4.2 Exploring Multispectral Backscatter Response Through Image-Based and Angular Range Analysis Approaches

Despite limitations associated with the use of uncalibrated backscatter data (Lurton and Lamarche, 2015; Schimel et al., 2018; Malik et al., 2019), the results provided basic information for interpretation of different seafloor types, and provided useful information on the acoustic response of the seabed. For most areas, the median uncalibrated backscatter values from the mosaics for all frequencies were low (slightly higher for lower frequency), which is characteristic of soft muddy deposits (Brown et al., 2019; Diesing et al., 2020). It is also worth noting that the characteristics of sub-bottom deposits can influence the acoustic response, especially for lower frequencies (Jackson and Richardson, 2007; Williams et al., 2009; Feldens et al., 2018). The acoustic response from sandy features (both for image-based and ARA results) is largely influenced by interface scattering, but could be further investigated by observing the influence of survey azimuth (Lurton et al., 2018), presence of bedforms, the variety of microtopography, and even more ground truthing to check lateral variability.

The use of multispectral technology offered increased seafloor discriminatory power based on the different frequency response of the seafloor across the frequency range, achieving a benthic prediction in agreement with earlier studies in this region (Quaresma et al., 2015; Vieira et al., 2019), and making it possible to improve the seafloor classification. Quaresma et al. (2020) found lower seabed density values in the shallow region close to the mud depocenter (**Figure 1**), and high density values (>1400 kg/m^3) in regions with depths greater than 30 m. Here, the lower uncalibrated backscatter values appear close to the steep feature (i.e., high slope–see **Figure 4**) and on the edge of the sandy elongated feature, where the bathymetric differences (**Figure 5**) between the frequencies reached up to 10 cm, indicating a mud accumulation partially driven by the seafloor morphology. In these regions, the lower frequency was presumably detecting the sub-surface sediment characteristics, while the higher frequency reflected primarily off the surface sediments of the seafloor, potentially indicating a thick, muddy deposit in this area. Although results from the bathymetric data (e.g., slope, ruggedness, bathymetric differences) played a secondary role compared to the backscatter here, they can serve as important predictors for seabed classification (Walbridge et al., 2018; Lucatelli et al., 2019), and some derivatives may be more important than bathymetry itself (Trzcinska et al., 2020).

The analysis of the composite band image proved to be an interesting tool to visualize the results in an integrated way, making it possible to observe regions where all frequencies indicated similar characteristics for distinct seabed types (for example, darker tones indicating more muddy bed, and whiter tones indicating more sandy sediment). Nevertheless, the observation of the RGB mosaic also allowed to recognize differences in acoustic responses in some regions, such as in the redder region near to the sample sites Doce 01 and Doce 02–indicating higher backscatter values for the lower frequency, and a lighter bluish region near to sample site Doce 11)–coloring that indicates higher backscatter values for the combination of the higher frequency bands (280 and 400 kHz). Quantifying the gain due the use of such methodology is beyond the scope of this work, but the result brings new information about the spectral signature of certain types of bottoms, and helps to consolidate the potential to improve the distinction and classification of the seafloor using multispectral backscatter (Costa, 2019).

Results from the GLCM analysis provide information that may aid in interpreting geoacoustic properties of the seabed. Jackson and Briggs (1992) found that the scattering interface may be a dominant factor controlling backscatter in sandy bottoms, while volume homogeneity is increasingly important in bottoms of higher mud (and lower medium-coarse sand) content. Here, the highest GLCM variance values were observed at the oblique and elongated sandy features, indicating higher uncalibrated backscatter values due to mosaic grey-level values—particularly

at the 280 kHz operating frequency (**Figure 10**). Hughes Clarke (2015) also noted an increase in backscatter intensity over sand sheets with increasing frequency, yet retained uncertainty regarding textural classification, as the bottom ruggedness measurement depends on the acoustic wavelength. Closer to the river mouth, differences in GLCM variance may be associated with other variables that influence the backscatter response, such as the thickness and homogeneity of the muddy subsurface deposit. In addition to informing classification, the GLCM variance contributed to visual interpretations, providing results that assist with backscatter analysis and classification of the seabed (Samsudin and Hasan, 2017; Runya et al., 2021).

While the 30–60° angular range is ideal for many seabed mapping applications (Lucieer et al., 2018), the utility of angular sector may change with frequency, and therefore, the extraction of backscatter values for different angular sectors may provide increased information with which to inform seabed classification. The 1–10° sector contains the most specular reflection, and here, appeared to show low contrast between different seabed types. The 11–20° data provided useful information at the fine sandy region, primarily at the higher frequencies. The angular response curves for this region show low backscatter loss for the first 20°, followed by a higher backscatter loss with increasing incidence angle. The 21–30° angles allowed for distinguishing bottom types using the lower frequencies. The 400 kHz data at these angles allows for visually distinguishing differences in bottom type close to the river mouth, which were not apparent at lower angles. The 31–40° sector showed high contrast between the sandy feature and the rest of the region. While the distinction between fine sand and muddy regions was not always clear using image-based methods, the use of backscatter at different angular sectors and frequencies enabled their discrimination, further indicating the benefits of combined analysis approaches for enhanced seafloor discrimination (Che Hasan et al., 2012; Ierodiaconou et al., 2018).

The ARA results appeared to correspond to the composition of sediment samples. Those with a large proportion of mud showed a greater rate of backscatter decrease with incidence angle than samples describing coarser sediments (**Figure 12**), and the greatest differences between frequencies. This trend was most apparent from the 400 kHz data, which is consistent with lower uncalibrated backscatter values mapped by the image-based results and with the acoustic influence of the muddy deposit homogeneity. Gaida et al. (2018) observed an increasingly flat angular response curve at 400 kHz in soft sediments compared to lower frequencies, which they attributed to an increased sensitivity to roughness at higher frequencies. Here, the angular response curves observed for sandy sample sites (Doce 07, 09, 11, and 12) exhibited flatter shape, similar to acoustic model curves (Applied Physics Laboratory, 1994). Combining with the other results, it can be concluded here that the flatter the angular response curve, the recognition of medium/coarse sandy bottoms is better observed in the image textural analysis, corroborating the greater influence of the scattering interface. Deriving consistent trends between backscatter and frequency over a range of seabed types remains difficult, yet Trzcinska et al. (2021) summarized backscatter values and angular response curves extracted from different studies over a range of seabed types. Multispectral backscatter facilitated this relationship with the results presented in the angular response curves: higher backscatter values were observed for higher frequencies in fine sand bottoms here, which appeared in a similar shape to the very fine sand in Trzcinska et al. (2021). Higher backscatter values for 280 kHz on a medium sand bottom here also appeared similar to their findings for sandy gravel (Trzcinska et al., 2021). For muddy bottoms, this relationship is made difficult by the suspected presence of a heterogeneous subsurface. For a better understanding of the results, it would certainly be interesting to include some subsurface analysis (e.g., sub bottom profiler or even subsurface sediment samples) and observe the ARA results at smaller angular intervals with more ground truthing.

The seafloor variability within the swath is one of the difficulties related to the angular range analysis, but the use of RGB image segmentation before clustering the variables of both approaches was an effective way to combine the methods and explore the dataset more adequately. The combination of such approaches applied to multispectral backscatter is still scarce in the scientific literature, but showed potential to better explore the advantages of each method using multifrequency dataset, even not involving bathymetric predictors.

5 CONCLUSION

Density-based clustering enabled the integration of results from multiple approaches to produce a comprehensive unsupervised classification of the seabed using multispectral acoustic data. Both image-based and ARA approaches produced input components for the final classification, and the combined use of both helped to ensure that all relevant information was included. While backscatter mosaics, the composite RGB and angular response curves potentially suggest two or three seabed classes, the final clustering identified two distinct acoustic seabed classes, with four subclasses within one of the broader classes, which corresponded closely with seafloor sediment samples collected at the site. In addition, angular range analysis suggested that information from different angular sectors may be informative for different seabed types, and using different frequencies. Therefore, multispectral backscatter appeared to offer greater advantages in terms of discrimination seafloor in mud and fine sand bottom types than in coarser sediments.

DATA AVAILABILITY STATEMENT

The raw data supporting the conclusion of this article will be made available by the authors, without undue reservation.

AUTHOR CONTRIBUTIONS

PM: field work, conceptualization, formal analysis, investigation, writing–original draft; AB and CB: conceptualization, review and

editing; BM: conceptualization, formal analysis, investigation, review and editing.

FUNDING

Data collection was carried out as part of Impactos Lama de Rejeito nos Habitat Marinhos da Foz do Rio Doce (FAPES Grant 77683390) and Environmental Monitoring Program (PMBA) (Fundação Renova-FEST-RRDM). This research is part of the Ocean Frontier Institute Benthic Ecosystem Mapping and Engagement (BEcoME) Project.

ACKNOWLEDGMENTS

PM was granted an international scholarship from the Coordenação de Aperfeiçoamento de Pessoal de Nível Superior–Brazil (CAPES)–Finance Code 001 at Dalhousie University to work in partnership in the Ocean Frontier Institute Benthic Ecosystem Mapping and Engagement (BEcoME) Project. AB is a Research Fellow of CNPq (PQ1D). We are grateful to all laboratory colleagues that collaborated during field working or helping in data processing and further discussions.

REFERENCES

Alevizos, E., and Greinert, J. (2018). The Hyper-Angular Cube Concept for Improving the Spatial and Acoustic Resolution of MBES Backscatter Angular Response Analysis. *Geosciences* 8, 446. doi:10.3390/geosciences8120446

Alevizos, E., Snellen, M., Simons, D., Siemes, K., and Greinert, J. (2018). Multi-angle Backscatter Classification and Sub-bottom Profiling for Improved Seafloor Characterization. *Mar. Geophys. Res.* 39, 289–306. doi:10.1007/s11001-017-9325-4

Amiri-Simkooei, A., Snellen, M., and Simons, D. G. (2009). Riverbed Sediment Classification Using Multi-Beam echo-sounder Backscatter Data. *J. Acoust. Soc. Am.* 126, 1724. doi:10.1121/1.3205397

Ankerst, M., Breunig, M. M., Kriegel, H.-P., and Sander, J. (1999). Optics. *SIGMOD Rec.* 28 (2), 49–60. doi:10.1145/304181.304187

Applied Physics Laboratory -, A. P. L. (1994). *APL-UW High-Frequency Ocean Environmental Acoustic Models Handbook*. Seattle, WA, USA: University of WashingtonApplied Physics Laboratory, University of Washington. Technical Report APL-UW TR9407.

Augustin, J. M., Le Suave, R., Lurton, X., Voisset, M., Dugelay, S., and Satra, C. (1996). Contribution of the Multibeam Acoustic Imagery to the Exploration of the Sea-Bottom. *Mar. Geophys. Researches* 18, 459–486. doi:10.1007/BF00286090

Bastos, A. C., Quaresma, V. S., Marangoni, M. B., D'Agostini, D. P., Bourguignon, S. N., Cetto, P. H., et al. (2015). Shelf Morphology as an Indicator of Sedimentary Regimes: A Synthesis from a Mixed Siliciclastic-Carbonate Shelf on the Eastern Brazilian Margin. *J. South Am. Earth Sci.* 63, 125–136. doi:10.1016/j.jsames.2015.07.003

Blondel, P., and Gómez Sichi, O. (2009). Textural Analyses of Multibeam Sonar Imagery from Stanton Banks, Northern Ireland continental Shelf. *Appl. Acoust.* 70, 1288–1297. doi:10.1016/j.apacoust.2008.07.015

Brooke, B. P., Nichol, S. L., Huang, Z., and Beaman, R. J. (2017). Palaeoshorelines on the Australian continental Shelf: Morphology, Sea-Level Relationship and Applications to Environmental Management and Archaeology. *Continental Shelf Res.* 134, 26–38. doi:10.1016/j.csr.2016.12.012

Brown, C., Beaudoin, J., Brissette, M., and Gazzola, V. (2019). Multispectral Multibeam Echo Sounder Backscatter as a Tool for Improved Seafloor Characterization. *Geosciences* 9 (3), 126. doi:10.3390/geosciences9030126

Brown, C. J., Smith, S. J., Lawton, P., and Anderson, J. T. (2011). Benthic Habitat Mapping: A Review of Progress towards Improved Understanding of the Spatial Ecology of the Seafloor Using Acoustic Techniques. *Estuarine, Coastal Shelf Sci.* 92 (3), 502–520. doi:10.1016/j.ecss.2011.02.007

Buscombe, D., and Grams, P. (2018). Probabilistic Substrate Classification with Multispectral Acoustic Backscatter: A Comparison of Discriminative and Generative Models. *Geosciences* 8 (11), 395. doi:10.3390/geosciences8110395

Campello, R. J. G. B., Moulavi, D., and Sander, J. (2013). "Density-Based Clustering Based on Hierarchical Density Estimates," in *Advances in Knowledge Discovery and Data Mining*. Editors J. Pei, V. S. Tseng, L. Cao, H. Motoda, and G. Xu, (Springer Berlin Heidelberg), 7819, 160–172. doi:10.1007/978-3-642-37456-2_14

Chakraborty, B., Menezes, A., Dandapath, S., Fernandes, W. A., Karisiddaiah, S. M., Haris, K., et al. (2015). Application of Hybrid Techniques (Self-Organizing Map and Fuzzy Algorithm) Using Backscatter Data for Segmentation and Fine-Scale Roughness Characterization of Seepage-Related Seafloor along the Western Continental Margin of India. *IEEE J. Oceanic Eng.* 40, 3–14. doi:10.1109/joe.2013.2294279

Che Hasan, R., Ierodiaconou, D., and Laurenson, L. (2012). Combining Angular Response Classification and Backscatter Imagery Segmentation for Benthic Biological Habitat Mapping. *Estuarine, Coastal Shelf Sci.* 97, 1–9. doi:10.1016/j.ecss.2011.10.004

Che Hasan, R., Ierodiaconou, D., Laurenson, L., and Schimel, A. (2014). Integrating Multibeam Backscatter Angular Response, Mosaic and Bathymetry Data for Benthic Habitat Mapping. *PLoS ONE* 9 (5), e9739. doi:10.1371/journal.pone.0097339

Cogan, C. B., Todd, B. J., Lawton, P., and Noji, T. T. (2009). The Role of marine Habitat Mapping in Ecosystem-Based Management. *ICES J. Mar. Sci.* 66 (9), 2033–2042. doi:10.1093/icesjms/fsp214

Comaniciu, D., and Meer, P. (2002). Mean Shift: A Robust Approach toward Feature Space Analysis. *IEEE Trans. Pattern Anal. Machine Intell.* 24 (5), 603–619. doi:10.1109/34.1000236

Costa, B. (2019). Multispectral Acoustic Backscatter: How Useful Is it for Marine Habitat Mapping and Management? *J. Coastal Res.* 35 (5), 1062. doi:10.2112/jcoastres-d-18-00103.1

Diesing, M., Mitchell, P. J., O'Keeffe, E., Gavazzi, G. O. A. M., and Bas, T. L. (2020). Limitations of Predicting Substrate Classes on a Sedimentary Complex but Morphologically Simple Seabed. *Remote Sensing* 12 (20), 3398. doi:10.3390/rs12203398

Diesing, M., Mitchell, P., and Stephens, D. (2016). Image-based Seabed Classification: What Can We Learn from Terrestrial Remote Sensing? *ICES J. Mar. Sci.* 73 (10), 2425–2441. doi:10.1093/icesjms/fsw118

Dominguez, J. M. L. (2006). The Coastal Zone of Brazil: An Overview. *J. Coastal Res.*, 16–20.

Ester, M., Kriegel, H., Sander, J., and Xu, X. (1996). "A Density-Based Algorithm for Discovering Clusters in Large Spatial Databases with Noise," in Proceedings of 2nd International Conference on Knowledge Discovery and Data Mining (Munich: Institute for Computer Science, University of Munich), 226–231. (KDD-96).

Fakiris, E., Blondel, P., Papatheodorou, G., Christodoulou, D., Dimas, X., Georgiou, N., et al. (2019). Multi-Frequency, Multi-Sonar Mapping of Shallow Habitats-Efficacy and Management Implications in the National Marine Park of Zakynthos, Greece. *Remote Sensing* 11, 461. doi:10.3390/rs11040461

Feldens, P., Schulze, I., Papenmeier, S., Schönke, M., and Schneider von Deimling, J. (2018). Improved Interpretation of Marine Sedimentary Environments Using Multi-Frequency Multibeam Backscatter Data. *Geosciences* 8 (6), 214. doi:10.3390/geosciences8060214

Fezzani, R., and Berger, L. (2018). Analysis of Calibrated Seafloor Backscatter for Habitat Classification Methodology and Case Study of 158 Spots in the Bay of Biscay and Celtic Sea. *Mar. Geophys. Res.* 39 (1–2), 169–181. doi:10.1007/s11001-018-9342-y

Fonseca, L., Brown, C., Calder, B., Mayer, L., and Rzhanov, Y. (2009). Angular Range Analysis of Acoustic Themes from Stanton Banks Ireland: A Link between Visual Interpretation and Multibeam Echosounder Angular Signatures. *Appl. Acoust.* 70 (10), 1298–1304. doi:10.1016/j.apacoust.2008.09.008

Fonseca, L., and Mayer, L. (2007). Remote Estimation of Surficial Seafloor Properties through the Application Angular Range Analysis to Multibeam

Sonar Data. *Mar. Geophys. Res.* 28 (2), 119–126. doi:10.1007/s11001-007-9019-4

Gaida, T., Tengku Ali, T., Snellen, M., Amiri-Simkooei, A., van Dijk, T., and Simons, D. (2018). A Multispectral Bayesian Classification Method for Increased Acoustic Discrimination of Seabed Sediments Using Multi-Frequency Multibeam Backscatter Data. *Geosciences* 8 (12), 455. doi:10.3390/geosciences8120455

Greene, H. G., Endris, C., Vallier, T., Golden, N., Cross, J., Ryan, H., et al. (2013). Sub-tidal Benthic Habitats of central San Francisco Bay and Offshore Golden Gate Area - A Review. *Mar. Geology*. 345, 31–46. doi:10.1016/j.margeo.2013.05.001

Hahsler, M., Piekenbrock, M., and Doran, D. (2019). Dbscan: Fast Density-Based Clustering with R. *J. Stat. Softw.* 91 (1). doi:10.18637/jss.v091.i01

Hahsler, M., and Piekenbrock, P. (2021). *Dbscan: Density Based Clustering of Applications with Noise (DBSCAN) and Related Algorithms*.

Haralick, R. M., Shanmugam, K., and Dinstein, I. H. (1973). Textural Features for Image Classification. *Syst. Man. Cybern. IEEE Trans.* 6, 610e621. doi:10.1109/tsmc.1973.4309314

Haris, K., Chakraborty, B., De, C., Prabhudesai, R. G., and Fernandes, W. (2011). Model-based Seafloor Characterization Employing Multi-Beam Angular Backscatter Data-A Comparative Study with Dual-Frequency Single Beam. *The J. Acoust. Soc. America* 130 (6), 3623–3632. doi:10.1121/1.3658454

Harris, P. T., and Baker, E. (2020). *Seafloor Geomorphology as Benthic Habitat: GeoHAB Atlas of Seafloor Geomorphic Features and Benthic Habitats*. 2nd ed. Elsevier.

Heap, A. D., Nichol, S. L., and Brooke, B. P. (2014). Seabed Mapping to Support Geological Storage of Carbon Dioxide in Offshore Australia. *Continental Shelf Res.* 83, 108–115. doi:10.1016/j.csr.2014.02.008

Hughes Clarke, J. E. (2015). *Multispectral Acoustic Backscatter from Multibeam, Improved Classification Potential*, 19. Maryland: U.S. Hydrographic Conference.

Ierodiaconou, D., Schimel, A. C. G., Kennedy, D., Monk, J., Gaylard, G., Young, M., et al. (2018). Combining Pixel and Object Based Image Analysis of Ultra-high Resolution Multibeam Bathymetry and Backscatter for Habitat Mapping in Shallow marine Waters. *Mar. Geophys. Res.* 39 (1–2), 271–288. doi:10.1007/s11001-017-9338-z

Innangi, S., Barra, M., Di Martino, G., Parnum, I. M., Tonielli, R., and Mazzola, S. (2015). Reson SeaBat 8125 Backscatter Data as a Tool for Seabed Characterization (Central Mediterranean, Southern Italy): Results from Different Processing Approaches. *Appl. Acoust.* 87, 109–122. doi:10.1016/j.apacoust.2014.06.014

Jackson, D. R., and Briggs, K. B. (1992). High-frequency Bottom Backscattering: Roughness versus Sediment Volume Scattering. *J. Acoust. Soc. America* 92 (2), 962–977. doi:10.1121/1.403966

Jackson, D. R., and Richardson, M. D. (2007). "High-frequency Seafloor Acoustics," in *Monograph Series in Seafloor Acoustics* (Springer), 616.

Kirkman, S. P., Holness, S., Harris, L. R., Sink, K. J., Lombard, A. T., Kainge, P., et al. (2019). Using Systematic Conservation Planning to Support Marine Spatial Planning and Achieve marine protection Targets in the Transboundary Benguela Ecosystem. *Ocean Coastal Manage.* 168, 117–129. doi:10.1016/j.ocecoaman.2018.10.038

Kriegel, H. P., Kröger, P., Sander, J., and Zimek, A. (2011). Density-based Clustering. *Wires Data Mining Knowl Discov.* 1 (3), 231–240. doi:10.1002/widm.30

Lamarche, G., and Lurton, X. (2018). Recommendations for Improved and Coherent Acquisition and Processing of Backscatter Data from Seafloor-Mapping Sonars. *Mar. Geophys. Res.* 39 (1–2), 5–22. doi:10.1007/s11001-017-9315-6

Le Bas, T. P. (2016). *RSOBIA - A New OBIA Toolbar and Toolbox in ArcMap 10.X for Segmentation and ClassificationGEOBIA 2016 : Solutions and Synergies. GEOBIA 2016 : Solutions and Synergies*. University of Twente Faculty of Geo-Information and Earth Observation ITC.

Le Quilleuc, A., Collin, A., Jasinski, M. F., and Devillers, R. (2021). Very High-Resolution Satellite-Derived Bathymetry and Habitat Mapping Using Pleiades-1 and ICESat-2. *Remote Sensing* 14 (1), 133. doi:10.3390/rs14010133

Lecours, V., Dolan, M. F. J., Micallef, A., and Lucieer, V. L. (2016). A Review of marine Geomorphometry, the Quantitative Study of the Seafloor. *Hydrol. Earth Syst. Sci.* 20 (8), 3207–3244. doi:10.5194/hess-20-3207-2016

Lee, S. T. M., Kelly, M., Langlois, T. J., and Costello, M. J. (2015). Baseline Seabed Habitat and Biotope Mapping for a Proposed marine reserve. *PeerJ* 3, e1446. doi:10.7717/peerj.1446

Lu, D., and Weng, Q. (2007). A Survey of Image Classification Methods and Techniques for Improving Classification Performance. *Int. J. Remote Sensing* 28 (5), 823–870. doi:10.1080/01431160600746456

Lucatelli, D., Goes, E. R., Brown, C. J., Souza-Filho, J. F., Guedes-Silva, E., and Araújo, T. C. M. (2019). Geodiversity as an Indicator to Benthic Habitat Distribution: An Integrative Approach in a Tropical continental Shelf. *Geo-Marine Lett.* doi:10.1007/s00367-019-00614-x

Lucieer, V., Roche, M., Degrendele, K., Malik, M., Dolan, M., and Lamarche, G. (2018). User Expectations for Multibeam echo Sounders Backscatter Strength Data-Looking Back into the Future. *Mar. Geophys. Res.* 39 (1–2), 23–40. doi:10.1007/s11001-017-9316-5

Lurton, X. (2010). *An Introduction to Underwater AcousticsPrinciples and Applications*. 2nd edition. UK: Springer Praxis Books & Praxis Publishing, 346.

Lurton, X., Eleftherakis, D., and Augustin, J.-M. (2018). Analysis of Seafloor Backscatter Strength Dependence on the Survey Azimuth Using Multibeam Echosounder Data. *Mar. Geophys. Res.* 39 (1–2), 183–203. doi:10.1007/s11001-017-9318-3

Lurton, X., and Lamarche, G. (2015). Backscatter Measurements by Seafloor-mapping Sonars. Guidelines and Recommendations. Available at: http://geohab.org/wp-content/uploads/2014/05/BSWG- REPORT-MAY2015.pdf.

Malik, M., Schimel, A. C. G., Masetti, G., Roche, M., Le Deunf, J., Dolan, M. F. J., et al. (2019). Results from the First Phase of the Seafloor Backscatter Processing Software Inter-comparison Project. *Geosciences* 9 (12), 516. doi:10.3390/geosciences9120516

Masetti, G., Mayer, L., and Ward, L. (2018). A Bathymetry- and Reflectivity-Based Approach for Seafloor Segmentation. *Geosciences* 8 (1), 14. doi:10.3390/geosciences8010014

McGonigle, C., and Collier, J. S. (2014). Interlinking Backscatter, Grain Size and Benthic Community Structure. *Estuarine, Coastal Shelf Sci.* 147, 123–136. doi:10.1016/j.ecss.2014.05.025

Montereale-Gavazzi, G., Roche, M., Lurton, X., Degrendele, K., Terseleer, N., and Van Lancker, V. (2018). Seafloor Change Detection Using Multibeam Echosounder Backscatter: Case Study on the Belgian Part of the North Sea. *Mar. Geophys. Res.* 39 (1–2), 229–247. doi:10.1007/s11001-017-9323-6

Mosca, F., Matte, G., Lerda, O., Naud, F., Charlot, D., Rioblanc, M., et al. (2016). Scientific Potential of a New 3D Multibeam Echosounder in Fisheries and Ecosystem Research. *Fish. Res.* 178, 130–141. doi:10.1016/j.fishres.2015.10.017

Parnum, I. M., and Gavrilov, A. N. (2011). High-frequency Multibeam echo-sounder Measurements of Seafloor Backscatter in Shallow Water: Part 2 - Mosaic Production, Analysis and Classification. *Uw Tech: Int. J Soc. Uw Tech.* 30 (1), 13–26. doi:10.3723/ut.30.013

Picard, K., Brooke, B. P., Harris, P. T., Siwabessy, P. J. W., Coffin, M. F., Tran, M., et al. (2018). Malaysia Airlines Flight MH370 Search Data Reveal Geomorphology and Seafloor Processes in the Remote Southeast Indian Ocean. *Mar. Geology*. 395, 301–319. doi:10.1016/j.margeo.2017.10.014

Quaresma, V. d. S., Catabriga, G., Bourguignon, S. N., Godinho, E., and Bastos, A. C. (2015). Modern Sedimentary Processes along the Doce River Adjacent continental Shelf. *Braz. J. Geol.* 45 (4), 635–644. doi:10.1590/2317-488920150030274

Quaresma, V. S., Bastos, A. C., Leite, M. D., Costa, A., Cagnin, R. C., Grilo, C. F., et al. (2020). The Effects of a Tailing Dam Failure on the Sedimentation of the Eastern Brazilian Inner Shelf. *Continental Shelf Res.* 205, 104172. doi:10.1016/j.csr.2020.104172

Rocha, G. A., Bastos, A. C., Amado-Filho, G. M., Boni, G. C., Moura, R. L., and Oliveira, N. (2020). Heterogeneity of Rhodolith Beds Expressed in Backscatter Data. *Mar. Geology*. 423, 106136. doi:10.1016/j.margeo.2020.106136

Runya, R. M., McGonigle, C., Quinn, R., Howe, J., Collier, J., Fox, C., et al. (2021). Examining the Links between Multi-Frequency Multibeam Backscatter Data and Sediment Grain Size. *Remote Sensing* 13 (8), 1539. doi:10.3390/rs13081539

Rzhanov, Y., Fonseca, L., and Mayer, L. (2012). Construction of Seafloor Thematic Maps from Multibeam Acoustic Backscatter Angular Response Data. *Comput. Geosciences* 41, 181–187. doi:10.1016/j.cageo.2011.09.001

Samsudin, S. A., and Hasan, R. C. (2017). "Assessment of Multibeam Backscatter Texture Analysis for Seafloor Sediment Classification," in *The International Archives of the Photogrammetry, Remote Sensing and Spatial Information Sciences*, XLII-4. doi:10.5194/isprs-archives-xlii-4-w5-177-2017

Schimel, A. C. G., Beaudoin, J., Parnum, I. M., Le Bas, T., Schmidt, V., Keith, G., et al. (2018). Multibeam Sonar Backscatter Data Processing. *Mar. Geophys. Res.* 39 (1–2), 121–137. doi:10.1007/s11001-018-9341-z

Sen, A., Ondréas, H., Gaillot, A., Marcon, Y., Augustin, J.-M., and Olu, K. (2016). The Use of Multibeam Backscatter and Bathymetry as a Means of Identifying Faunal Assemblages in a Deep-Sea Cold Seep. *Deep Sea Res. Oceanographic Res. Pap.* 110, 33–49. doi:10.1016/j.dsr.2016.01.005

Simons, D. G., and Snellen, M. (2009). A Bayesian Approach to Seafloor Classification Using Multi-Beam echo-sounder Backscatter Data. *Appl. Acoust.* 70, 1258–1268. doi:10.1016/j.apacoust.2008.07.013

Smith Menandro, P., and Cardoso Bastos, A. (2020). Seabed Mapping: A Brief History from Meaningful Words. *Geosciences* 10 (7), 273. doi:10.3390/geosciences10070273

Stephens, D., and Diesing, M. (2014). A Comparison of Supervised Classification Methods for the Prediction of Substrate Type Using Multibeam Acoustic and Legacy Grain-Size Data. *PLoS ONE* 9 (4), e93950. doi:10.1371/journal.pone.0093950

Stewart, H. A., and Jamieson, A. J. (2019). The Five Deeps: The Location and Depth of the Deepest Place in Each of the World's Oceans. *Earth-Science Rev.* 197, 102896. doi:10.1016/j.earscirev.2019.102896

Tamsett, D., McIlvenny, J., and Watts, A. (2016). Colour Sonar: Multi-Frequency Sidescan Sonar Images of the Seabed in the Inner Sound of the Pentland Firth, Scotland. *Jmse* 4 (1), 26. doi:10.3390/jmse4010026

Trzcinska, K., Janowski, L., Nowak, J., Rucinska-Zjadacz, M., Kruss, A., von Deimling, J. S., et al. (2020). Spectral Features of Dual-Frequency Multibeam Echosounder Data for Benthic Habitat Mapping. *Mar. Geology.* 427, 106239. doi:10.1016/j.margeo.2020.106239

Trzcinska, K., Tegowski, J., Pocwiardowski, P., Janowski, L., Zdroik, J., Kruss, A., et al. (2021). Measurement of Seafloor Acoustic Backscatter Angular Dependence at 150 kHz Using a Multibeam Echosounder. *Remote Sensing* 13 (23), 4771. doi:10.3390/rs13234771

Vieira, F. V., Bastos, A. C., Quaresma, V. S., Leite, M. D., Costa, A., Oliveira, K. S. S., et al. (2019). Along-shelf Changes in Mixed Carbonate-Siliciclastic Sedimentation Patterns. *Continental Shelf Res.* 187, 103964. doi:10.1016/j.csr.2019.103964

Walbridge, S., Slocum, N., Pobuda, M., and Wright, D. (2018). Unified Geomorphological Analysis Workflows with Benthic Terrain Modeler. *Geosciences* 8 (3), 94. doi:10.3390/geosciences8030094

Williams, K. L., Jackson, D. R., Dajun Tang, D., Briggs, K. B., and Thorsos, E. I. (2009). Acoustic Backscattering from a Sand and a Sand/Mud Environment: Experiments and Data/Model Comparisons. *IEEE J. Oceanic Eng.* 34 (4), 388–398. doi:10.1109/joe.2009.2018335

Yizong, C. (1995). Mean Shift, Mode Seeking, and Clustering. *IEEE Trans. Pattern Anal. Machine Intell.* 17, 790–799. doi:10.1109/34.400568

Conflict of Interest: The authors declare that the research was conducted in the absence of any commercial or financial relationships that could be construed as a potential conflict of interest.

Publisher's Note: All claims expressed in this article are solely those of the authors and do not necessarily represent those of their affiliated organizations, or those of the publisher, the editors and the reviewers. Any product that may be evaluated in this article, or claim that may be made by its manufacturer, is not guaranteed or endorsed by the publisher.